

The last 5 Gyr of Galactic chemical evolution based on H II region abundances derived from a temperature independent method

Leticia Carigi¹

carigi@astro.unam.mx

Manuel Peimbert¹

peimbert@astro.unam.mx

and

Antonio Peimbert¹

antonio@astro.unam.mx

ABSTRACT

Most of the chemical evolution models are not very reliable for the last 5 Gyr of galactic evolution; this is mainly because abundance gradients found in the literature show a big dispersion for young objects; a big culprit of this is the dispersion found in H II region gradients. Part of this dispersion arises from two different methods used to determine O/H in H II regions: the direct method (DM), based on forbidden lines; and the temperature independent method (TIM), based on permitted lines; the differences between these two methods are about 0.25 dex. We present two chemical evolution models of our galaxy to fit the O/H gradients of H II regions, one obtained from the DM and the other obtained from the TIM. We find that the model based on the TIM produces an excellent fit to the observational stellar constraints (B-stars, Cepheids, and the Sun), while the model based on the DM fails to reproduce them. Moreover the TIM model reproduces the flattening observed in the 3 – 6 kpc galactocentric range; this flattening is attained with an inside-out star formation quenching in the inner disk starting ~ 9 Gyr ago.

Subject headings: H II regions– ISM: abundances

¹Instituto de Astronomía, Universidad Nacional Autónoma de México, Apdo. Postal 70-264, México, C.P. 04510, CdMx, Mexico

1. Introduction

Our knowledge of the Milky Way (MW) is considerably wider and deeper than our knowledge of any other galaxy; consequently the MW should be used as a benchmark for the study of other galaxies. Therefore, it is paramount to have a reliable and robust model of the Galaxy to improve the development of future models of other galaxies; a key ingredient to produce meaningful models is to have significant observational restrictions of high quality.

Furthermore, a precise chemical evolution model for the MW is important because, by trying to reproduce the observed abundances (particularly the new determinations achieved with 8-10 m-class telescopes; e.g. García-Rojas et al. 2006; Martin et al. 2015; Esteban et al. 2017), we can put constraints on the many parameters involved in the formation and evolution of the MW.

Most of the effort, of the chemical evolution models of the Galactic disk found in the literature, has been placed on fitting the observed radial distribution of M_{gas} , of M_{stars} , and of the SFR. The chemical gradients of HII regions have not been used as robust observational constraints because, while the slope of the chemical gradient is not controversial, the absolute O/H values of the HII region gradients found in the literature present a big dispersion; this becomes more pronounced when combined with gradients derived from other types of objects (such as B-stars, cepheids, PNe, etc.). Therefore, to constrain the chemical enrichment, some models fit the observed [O/Fe] - [Fe/H] trend shown by stars at the solar neighbourhood (e.g. Renda et al. 2005; Mollá et al. 2015), and others focus on normalizing their results to the solar abundances at the Sun’s age (e.g. Romano et al. 2010; Minchev et al. 2013; Prantzos 2016).

It is known that the Sun might have migrated away from its birth galactocentric distance (e.g. Wielen, Fuchs, & Dettbarn 1996; Portegies Zwart 2009) and detailed dynamical evolution models of the MW provide a restriction for the birth place of the Sun given by $6.3 \lesssim R \lesssim 9.1$ kpc (Martínez-Medina et al. 2017)

The O/H gradient is obtained from young objects assuming that they are representative of their present R value. Therefore we use H II regions, early type main sequence B stars, and young Cepheids (all objects with ages smaller than 200 Myr) to determine the O/H values. These objects are very young and we do not expect them to have experienced important migrations since their birth. Unfortunately O/H values derived by different techniques and authors show very large dispersions (higher than 1.0 dex; see, for example, fig. 4 in Kubryk et al. 2015a).

In the specific case of the O/H gradients derived from H II regions; there are two different strategies to derive O/H values: a) those based on the direct method (DM) where

the O^{++}/H^+ values are derived from the forbidden lines of O^{++} , and the temperature of the O^{++} region from the ratio of the auroral (4363 Å) to nebular (5007 Å) emission lines (e.g. Fernández-Martín et al. 2017; Esteban & García-Rojas 2018), and b) those based on a temperature independent method (TIM) where the O^{++}/H^+ values are derived from the recombination lines of O^{++} and H^+ (e.g. Esteban et al. 2005).

The difference arises because the DM is very sensitive to the temperature and in the presence of temperature inhomogeneities only provides a lower limit to the O/H ratio (Peimbert 1967; Peimbert & Costero 1969). A more accurate method to obtain the O/H ratio is based on the recombination lines (RLs) of O because their temperature and density dependences are similar to those of the H RLs and nearly cancel out, making the O/H ratio practically temperature and density independent.

The problem with the TIM is that the intensities of the O II RLs are difficult to obtain: a) they are about three to four orders of magnitude fainter than the [O III] nebular lines and about one order of magnitude fainter than the [O III] auroral lines, and b) to obtain accurate O II intensities requires high spectral resolution; these difficulties imply that, to obtain TIM abundances, observations with large telescopes are required. Overall this method is seldom used and most determinations in the literature are based on O forbidden lines (FLs).

Alternatively, Peimbert (1967) and Peimbert & Costero (1969) presented a formalism to correct the chemical abundances determined using CELs in the presence of thermal inhomogeneities; this correction is possible for objects where the temperature dispersion can be estimated. This is called the t^2 formalism and the t^2 value is a measure of the temperature dispersion. One way to obtain a t^2 value is to compare FL temperatures with either H I or He I temperatures; unfortunately good H I and He I temperatures are available for only a few objects, usually only for those where O II RL abundances are available.

Recent reviews on the determination of abundances based on the DM and on the TIM have been presented by Pérez-Montero (2017) and Peimbert et al. (2017) respectively.

One of the goals of this paper is to select carefully the data to have a smaller dispersion on the O/H values and to obtain a meaningful O/H gradient. A special effort will be made in the determination of the O/H abundance ratios in H II regions because these objects are the most recent and are not affected by migration; there are systematic differences in the O/H values that amount typically to about 0.25 dex between the two most popular methods; one issue that we are going to tackle is which of those two methods is better suited to model the MW.

The main objective of this paper is to present a new Galactic model of chemical evolution able to reproduce the best observational data; specifically a model capable of simultaneously

fitting the data provided by H II regions, Cepheids, B stars, and the Sun; such model will improve our understanding of the chemical evolution of the Galactic disk, specially of the last 5 Gyrs.

2. O/H values determined from H II regions

We are looking for objects with high quality observations, preferably observed with 8-10m class telescopes; we found 10 H II regions for which oxygen RLs are measured, all of them observed with the Ultraviolet/Visible Echelle Spectrograph (UVES) at the 8.2m Very Large Telescope (VLT); since most of these stars are inside the solar circle, we have extended this sample with 9 H II regions observed with long slit spectrographs with the 10.4m Gran Telescopio de Canarias (GTC), mostly outside the solar circle; we also included 2 H II regions observed with the 4.2m William Herschel Telescope (WHT). The entire set is presented in Table 1.

Recently, Esteban & García-Rojas (2018) published a sample with additional data in the internal part of the Galaxy. However, the highest O^{++} fraction of such sample is 0.27 dex while the sample by Peña-Guerrero et al. (2012) only has two objects with O^{++} below 0.27 dex and, since the determinations of Peña-Guerrero et al. rely heavily on O^{++} data, the calibration of low ionization objects would be suspect; also this new sample is much fainter than the sample we are using (the typical errors in O/H for our sample are ~ 0.04 dex while the errors in the new sample are closer to 0.08 dex); consequently we have not used these data.

2.1. Direct method

In Table 1 we present the O/H gaseous abundances derived from forbidden lines under the assumption that there are no temperature inhomogeneities, $(O/H)_{FL}$. We also present the correction to these abundances due to the fraction of O atoms trapped in dust grains in H II regions, $(O/H)_{FL} + DUST$. The fraction of O trapped into dust grains depends slightly on metallicity, and for these chemical abundances is in the 0.10 to 0.11 dex range (Peimbert & Peimbert 2010).

In Figure 1a we present two straight lines to fit the data. For the 4 to 10 kpc range the slope amounts to -0.0170 dex/kpc, while for the 9.5 to 17.5 kpc range the slope amounts to -0.0629 dex/kpc. In Figure 1b we present a parabolic fit to the O/H values derived from the DM. The parabolic fit for the $\log O/H$ versus R data is better than the linear one. The

equation for the parabolic fit is:

$$12 + \log O/H = 8.571 + 0.0325 \left(\frac{R}{\text{kpc}} \right) - 0.00353 \left(\frac{R}{\text{kpc}} \right)^2. \quad (1)$$

2.2. Temperature independent method

In Table 2 we present the O/H gaseous abundances derived from RLs, $(O/H)_{\text{RL}}$. We also present the correction to these abundances due to the fraction of O atoms trapped in dust grains $(O/H)_{\text{RL}} + \text{DUST}$ (Peimbert & Peimbert 2010). They are the best observed H II regions and comprise a set of 10 objects.

For objects where no RLs are available, no true TIM abundances can be obtained, however it is possible to correct for an average abundance discrepancy factor, ADF, for objects where only FL abundances are available (e.g. Peña-Guerrero et al. 2012; Peimbert et al. 2017, and references therein).

In Table 3 we present a set of 11 H II regions where in column 3 we include again the $(O/H)_{\text{FL}}$ values for these objects. Also in column 4 of this Table we include the $(O/H)_{\text{TOTAL}}$ values where we have adopted the calibration by Peña-Guerrero et al. (2012) to correct for the presence of dust and temperature inhomogeneities in this set of objects. The correction by Peña-Guerrero et al. was determined by fitting the dependence of the ADF to both O/H and O^{++}/O ; in that work it was found that the correction has a weak dependence with metallicity and a negligible dependence with degree of ionization. For this set of objects corrections are in the 0.19 to 0.22 dex range.

In Figure 2 we include the set of 10 objects where the $(O/H)_{\text{TOTAL}}$ values were obtained from the RLs, and the set of 11 objects where the $(O/H)_{\text{TOTAL}}$ were obtained from the $(O/H)_{\text{FL}}$ values and the calibration by Peña-Guerrero et al. (2012).

In Figure 2a we present the O/H values for the galactic H II regions based on the TIM. Also in Figure 2a we present two pairs of lines to fit the data for the 4 to 10 kpc range the slope amounts to -0.0263 dex/kpc and for the 9.5 to 17.5 kpc range the slope amounts to -0.0638 dex/kpc. In Figure 2b we present a parabolic fit to the O/H values derived from the TIM. The parabolic fit for the log O/H versus R data is better than the linear one. The equation for the parabolic fit is:

$$12 + \log(O/H) = 8.888 + 0.0142 \left(\frac{R}{\text{kpc}} \right) - 0.00289 \left(\frac{R}{\text{kpc}} \right)^2. \quad (2)$$

Based on this equation, it is possible to compare the observed slopes by other authors and compare them with our observations (see Table 4).

From Figures 1 and 2 and equations (1) and (2) it can be seen that H II regions show a flattening of the O/H gradient that increases from the outer parts to the inner parts of the Galaxy, the 18 to 6 kpc range.

3. O/H values determined from other objects

3.1. Comparison with the early B type stars in the Orion Nebula

From 13 B0 V to B2 V stars of the Orion OB 1 association Nieva & Simón-Díaz (2011) obtain that $12 + \log(\text{O}/\text{H}) = 8.77 \pm 0.03$; later on, from B-stars located at distances from the Sun smaller than 350 pc, Nieva & Przybilla (2012) find $12 + \log(\text{O}/\text{H}) = 8.76 \pm 0.05$. Both results are far from the 8.59 dex value obtained by the DM, but in excellent agreement with the 8.80 obtained from equation (2) and the 8.76 ± 0.04 value obtained from the TIM for the Orion nebula by Esteban et al. (2004).

3.2. Early B type stars

In Figure 3 we present a set of 18 O/H values in the 6-18 kpc range obtained from 51 early type B-stars of Galactic, open cluster associations by Rolleston et al. (2000). The distances to these associations are well known and their stars are younger than 100 Myr, therefore these abundances should be representative of the present ISM values. We also present 4 B-stars, studied by the same group, with galactocentric distances in the 2-5 kpc range (Smartt et al. 2001).

3.3. Cepheids

The Cepheids used in this paper are Type I or classical, which are younger than 200 Myr, and consequently can be compared, both chemically and dynamically, with H II regions and main sequence early B type stars.

In Figure 3 we present also a set of 397 disk Cepheids compiled by Martin (private communication, 2017) based on data by his Andrievsky’s group (Luck et al. 2013; Korotin et al. 2014; Martin et al. 2015; Andrievsky et al. 2016). From this figure we conclude that the O/H values derived with the TIM are in reasonable agreement with the O/H values of the Cepheids and B-stars, on the other hand the O/H values derived from the DM are typically from 0.2 to 0.3 dex smaller than those derived with early type B-stars and disk Cepheids.

3.4. Combined Fit

Since the three sets of O/H data: H II regions, early B-stars, and Cepheids are in reasonable agreement, we also present a fit which combines the three sets to have an observational constraint on the O/H values for different galactocentric distances. The most direct way of doing so is to simultaneously fit all the observed data points regardless of their origin; this would be a good approach if all the data points had the same origin, or had the same systematic errors. However, we are dealing with three different sets of data that probably present different systematics; also there are enough data points in the samples so the errors should be dominated by the systematic errors within each method and not due to the statistical errors within the sample. Therefore we consider that each data set should be treated independently; and then the fits should be averaged giving each set an equal weight.

In Figure 4 we present the O/H data provided by Cepheids, B-stars, and H II regions using the TIM. We also present the parabolic fit to the three sets of data giving to each set one third of the weight. The parabolic weighted fit is given by:

$$12 + \log(\text{O/H}) = 8.952 + 0.0033 \left(\frac{R}{\text{kpc}} \right) - 0.00245 \left(\frac{R}{\text{kpc}} \right)^2. \quad (3)$$

This fit is very similar to that given by equation (2), and since this paper is centered in H II regions we will use equation (2) to fit the chemical evolution models.

4. Chemical evolution models for the disk of the Galaxy

We present three chemical evolution models for the Galactic disk. All these models were built to reproduce three present-time observational constraints along the Galactic disk: the distributions of the total baryonic mass, $M_{tot}(R)$, the gas mass, $M_{gas}(R)$, and the O/H values for H II regions between $5 < R(\text{kpc}) < 17$.

Based on observations, $M_{tot}(R) = 50e^{-(R-8)/R_{disk}}$ (Fenner & Gibson 2003), where the disk scalelength, R_{disk} , ranges between 2.3 and 5 kpc for different spectral bands (Yin et al. 2009); for our models, R_{disk} is a free parameter determined to reproduce the slope of the O/H gradient for $R > 12$ kpc. The observed $M_{gas}(R)$ values are obtained by adding the atomic and molecular data from fig. 7 by Kennicutt & Evans (2012). These $M_{gas}(R)$ values include the hydrogen and helium components.

The age of the models is 13 Gyr and the Sun formed at $t = 8.4$ Gyr in the solar vicinity, which is located in a ring of 8-kpc-medium radius and with an 0.5-kpc width. The MW disk started to form at $t = 1$ Gyr in an inside-out scenario of primordial infall with time-scales

$\tau_{disk} = (R/kpc - 2)$ Gyr (Chiappini et al. 1997). The halo formed during the first Gyr of the evolution with a constant timescale $\tau_{halo} = 0.5$ Gyr (see Figure 5).

The star formation rate is a spatial and temporal function of the form $SFR(R, t) = \nu(R, t) \times Mtot^{0.4}(R, t) \times Mgas^{1.4}(R, t)$, where $Mtot = Mgas + Mstar$ (Matteucci & Chiappini 1999). The values of $\nu(R, t)$ that we choose are those that reproduce the general behavior of $Mgas(R)$ and the flattening of the O/H radial gradient for $R \leq 5$ kpc. The initial mass function is that by Kroupa et al. (1993) in the $0.08 - Mup M_{\odot}$ range, where Mup is a free parameter, that is obtained by matching the absolute value of the observed O/H gradient.

The metal-dependent yields for $m < 8 M_{\odot}$ were taken from Marigo et al. (1996, 1998) and Portinari et al. (1998) and for $m > 8 M_{\odot}$ from Hirschi (2007), Meynet & Maeder (2002), and Maeder (1992, high mass loss rate model). Since the Fe yields are not computed by the Geneva group, we adopted the Woosley & Weaver (1995) values, following the Carigi & Hernandez (2008) prescription. For binary stars ($3 < mbin(M_{\odot}) < 16$), we adopted the yields by Nomoto et al. (1997) for type Ia supernovae by using the formulation by Greggio & Renzini (1983). We considered $A_{bin} = 0.066$, as the fraction of binary stars that become SNIa progenitors.

The three models focus on $R > 3$ kpc, therefore the Galactic bar and bulge are not considered, and no galactic winds are assumed.

Two of these models (CP11 and TIM) were built to reproduce the observed O/H values based on the temperature independent method determinations (Figures 6 and 7) and the third model (DM) was built to reproduce the O/H values of the H II regions derived from the direct method (Figures 8 and 9).

4.1. Astrophysical choices for the ingredients of the models

As most representative works on chemical evolution models for spiral galaxies, we adopt an inside-out formation scenario for the Galactic disk. Mollá et al. (2016) computed different infall rates for 16 theoretical galaxies with virial masses between 5×10^{10} and $10 \times 10^{13} M_{\odot}$; they concluded that the initial infall rate is greater, yet decreases more rapidly, in the inner disk; thus agreeing with the inside-out escenario and with cosmological simulations. In a recent work, Nuza et al. (2018) studied the infall R and t dependencies in 4 simulated MW-like galaxies; they found that the inner disks assemble in shorter times than the outer disks, as the inside-out scenario predicts. Also, the metallicity distribution function observed by APOGEE at different Rs (Hayden et al. 2015) suggest an inside-out formation.

In our models, we consider the well known Kennicutt-Schmidt law, $SFR(R, t) \propto Mgas^{1.4}(R, t)$, obtained empirically for spiral galaxies (Kennicutt 1998). The proportionality coefficient we use is given by $(Mgas + Mstar)^{0.4}$, and can be approximated by $Mstar^{0.4}$ (since $Mgas \ll Mstar$ for most of the evolution). Recently Shi et al. (2018) presented a revision of the Schmidt law based on spatially resolved SFR, $Mgas$, and $Mstar$ from dwarf, merging, and spiral galaxies. They found the star formation efficiency in galaxies depends on the stellar mass surface density, as $Mstar^{0.5}$, very similar to ours.

Romano et al. (2005) tested several IMFs and concluded that the Kroupa et al. (1993) IMF reproduces many important constraints of the solar vicinity, and hence, is the one used in our models. Romano et al. (2010) showed a comparative study among different stellar yields, and concluded that the high wind yields improve the model predictions. Moreover, they mentioned other independent and successful chemical evolution models that considered yield sets for massive stars similar to those assumed in our CEMs.

More recently Berg et al. (2016) studied the C/O-O/H trend in dwarf galaxies together with that shown by stars of the solar vicinity. They compared these trends with the C/O-O/H relation predicted by independent CEMs that considered different combinations of stellar yields and IMFs. In that work, Berg et al. concluded that “The Carigi & Peimbert model [our CP11 model] is the most successful at reproducing the general trend seen for the collective $\log(C/O)$ data over the observed range in oxygen abundance”.

4.2. CP11 Model

The CP11 model corresponds to the high wind yield model by Carigi & Peimbert (2011). They considered the yields computed from high stellar wind for massive stars of high metallicity. Based on the O/H data from the TIM, obtained before 2011 and that only included objects in the 6-11 kpc range, Carigi and Peimbert concluded that the best model was the one that assumed a moderate mass loss rate for massive stars of solar metallicity, given by the average of the high and low wind models. However, the high wind model reproduces better the new O/H data derived by the TIM presented in this paper (See Figure 5). The high wind yield model by CP11 considered $Rdisk = 3.5$ kpc, $Mup = 80 M_{\odot}$, and $\nu = 0.019$ as a spatial and time constant. Carigi & Peimbert (2008, 2011) presented very good fits to the high wind model with the C/H and C/O gradients as well as with the C/O-O/H, C/Fe-Fe/H, O/Fe-Fe/H, and time-Fe/H evolutionary trends at the solar vicinity. In Figures 6, 7, and 10 it can be noted the good agreements of this model with the current observational data. In Figure 11 (left panels) we show the evolution of the O/H values and the SFR.

4.3. TIM model

This model is identical to the CP11 model, except on the star formation history for $R < 6$ kpc. To reproduce the O/H flattening ($12+\log(\text{O}/\text{H}) \sim 8.83$, see Figure 6) we assume a unit step function, such that diminishes abruptly the $SFR(R)$ at specific times (quenching times) as a function of R . Then we adopt the current star formation rate observed at these radii (Kennicutt & Evans 2012) for the rest of the evolution. For $R = 3, 4,$ and 5 kpc, the observed SFR is equal to $0.45, 0.55,$ and $0.65 \text{ M}_{\odot}\text{pc}^{-2}\text{Gyr}^{-1}$, respectively, see Figure 10. We ran several models, testing different quenching times, where we chose the highest times that match $12+\log(\text{O}/\text{H}) \sim 8.83$. In Figure 11 (central panels), the decrease of the SFR and its effect on O/H can be noted, specifically, for $R = 3, 4,$ and 5 kpc the quenching times are $4.08, 6.10,$ and 8.38 Gyr, respectively.

In Figure 6 we present the model built to reproduce the O/H values of H II regions derived from the TIM and corrected by dust depletion. For $R < 6$ kpc the TIM model presents a flat gradient emulating a quasi flat behavior shown by H II regions. This flattening is a consequence of the assumptions of an inside-out reduction of the star formation rate. The abundances predicted by the TIM model only differ from those by CP11 in the 3-6 kpc range. For comparison, we also plot the abundances from the CP11 model.

In Figure 7a we compare the O/H radial distribution in the interstellar medium at present time, obtained by the TIM and CP11 models, with B-stars of Galactic open cluster associations by Rolleston et al. (2000) at different R , with the O/H average of B-stars in the solar vicinity by Nieva & Przybilla (2012), as well as with individual B-stars near the centre of the Galaxy ($2.5 \leq R \leq 4.7$ kpc) from Smartt et al. (2001). Since these stars are of spectral type B0 V to B2 V, they have been recently formed; and, consequently, their chemical abundances should be representative of the current O/H values in the interstellar medium. We find that in general both models are in good agreement with the observations, however the TIM model produces a slightly better fit for $R < 6$ kpc, since this model is in agreement, at one sigma, with all the values for $R \leq 4.7$ kpc.

In Figure 7b we compare the current O/H radial distribution from both models, with the Cepheid data. As B-stars, Cepheids are young stars (younger than 200 Myr), and we expect their abundances to be representative of the current ISM. We find that the values predicted by the TIM and CP11 models are similar to those of these stars. However, for the inner disk, the CP11 model matches better the few observations for $R < 6$ kpc. More data are needed to discriminate between both models.

In Figure 7c we present the predicted O/H radial distribution at 8.4 Gyr, the evolutionary-time when the Sun was formed. We consider that the age for the Sun is 4.6 Gyr and the solar

initial O/H value is the protosolar value, $12 + \log(\text{O}/\text{H}) = 8.73 \pm 0.05$, by Asplund et al. (2009). The galactocentric distance at which the Sun was born is not known, but recent dynamical models for the solar orbit predict a value of 7.7 ± 1.4 kpc at one sigma for the solar origin (Martínez-Medina et al. 2017). The spatial, temporal and O/H agreements with the model are excellent. Therefore, the model does not need to invoke a radial migration of the Sun to explain its chemical properties.

To estimate the birth radius of the Sun, we compare the protosolar abundance, $12 + \log(\text{O}/\text{H}) = 8.73 \pm 0.05$ (Asplund et al. 2009), with the chemical abundances produced by our models 4.6 Gyr ago. Specifically, O/H abundances of 8.68 and 8.78 are achieved at $R = 8.7$ and $R = 6.3$ kpc in both the TIM and CP11 models, see Figure 7c. Moreover, the dynamic models by Martínez-Medina et al. (2017) indicate that the Sun may have been born between 6.3 and 9.1 kpc. Therefore, we estimate that the Sun originated between 6.3 and 8.7 kpc and that the Sun may have migrated between 1.7 kpc outwards and 0.7 kpc inwards, to its present location.

Our determination of the birth radius of the Sun is in agreement, at one sigma, with those obtained from chemodynamical models by Minchev et al. (2013) (4.4 to 7.7 kpc) and by Kubryk et al. (2015a) (6.8 kpc) but slightly higher than the value mentioned by Nieva & Przybilla (2012) (5 to 6 kpc).

4.4. DM Model

Since the ratios between O/H values determined from TIM and DM are nearly constant (i.e. there is no clear radial trend in the observed ADFs), we apply the same idea and procedure of quenching for both models. Because the O/H flattening value is lower from the DM, and the SFR is higher at the inner galactocentric radii from the inside-out scenario, we impose a SFR quenching at earlier times for the DM model. Specifically, to reproduce the O/H flattening ($12 + \log(\text{O}/\text{H}) \sim 8.7$) for $R = 3, 4,$ and 5 kpc, the quenching times are 3.30, 3.50 and 5.40 Gyr, respectively. See Figures. 8, 9, 10, and 11 (right-bottom panel).

Since the O/H values from the DM are lower by ~ 0.25 dex than those from the TIM model, the DM model needs a smaller amount of stars to produce O, consequently an $M_{\text{up}} = 40 M_{\odot}$ is required. Similarly to obtain a better match for the O/H values with $R > 12$ kpc a value for $R_{\text{disk}} = 4.5$ kpc is required.

Similarly to the previous section, in Figures 8 and 9, we present the results of the model built to reproduce the O/H values of the H II regions derived from the DM.

The flat behavior shown by H II regions in the 5 to 8 kpc range (see Figure 8), can be theoretically reproduced by an earlier inside-out reduction of the star formation rate (see Figure 11). In Figure 9 (panels a and b) we compare the current O/H vs R relation from the model with the O/H values from B-stars and Cepheids, respectively. It can be noted that the agreement between the observed O/H values and the model is poor, being about 0.25 dex lower than observed. In Figure 9c, the predicted initial solar value, $12 + \log \text{O/H}$, is in the 8.40 to 8.56 range, about 0.25 dex smaller than the initial solar value that amounts to 8.73 Asplund et al. (2009). No migration (outwards or inwards) can explain the O/H solar value, without reducing the solar age. In an extreme case, had the Sun been born at $R \sim 6$ kpc, the O/H value of the ISM at $R = 6$ kpc reaches ~ 8.73 dex at $t \sim 12$ Gyr (see Figure 11), this would imply a solar age of ~ 1 Gyr, in contradiction with the accepted value of 4.6 Gyr.

5. Discussion

A fundamental problem to make successful CEMs is to choose which observational data to fit to the models. In this work we are focusing on the long standing problem of whether DM or TIM abundances should be used as observational restrictions. Robles-Valdez et al. (2013) find for M33 that, on average, H II region DM abundances are ~ 0.34 dex smaller than those of B-supergiants; while H II region abundances corrected by t^2 (equivalent to the TIM) are consistent with the stellar and RL abundances. Alternatively, Bresolin et al. (2009) find, for NGC 300, that CEL abundances agree better with abundances derived from AB supergiants. Toribio San Cipriano et al. (2016) observe both galaxies and find, again, a better agreement for RLs in M33 and a better agreement for CELs in NGC 300. Bresolin et al. (2016) suggest that DM abundances agree better with the AB supergiant abundances at sub-solar metallicities, while at super-solar metallicities RLs agree better with the supergiant data. Our result agrees with Robles-Valdez et al.; we find that DM abundances fall short of stellar abundances in the MW for H II regions between 5 and 17 kpc (equivalent to $8.3 \lesssim 12 + \log(\text{O/H}) \lesssim 8.88$).

All these observations should be used to restrict the several inputs and free parameters of the CEMs. The chemical history of the CP11 and TIM models have been successfully tested in the solar vicinity (see Carigi & Peimbert 2008, 2011) because in our neighborhood the number of observational constraints is similar to the number of free parameters of the CEMs, (i.e., infall, SFR, IMF, and stellar yields; see Section 4).

As we mention in the Section 4: the upper mass limit, M_{up} , of the initial mass function is a free parameter of the chemical evolution models, that is obtained mainly from the

absolute H II region O/H values. Since the O/H values in the Galactic disk determined from the TIM are ~ 0.25 dex higher than those obtained from the DM, and O is produced mainly by massive stars, the CP11 and TIM models require an $M_{up} = 80 M_{\odot}$, while the DM model requires an $M_{up} = 40 M_{\odot}$.

Similar M_{up} values were found by Hernández-Martínez et al. (2011) for NGC 6822, an irregular galaxy of the Local Group. Their chemical evolution model built to reproduce O/H values determined from recombination lines (or TIM, in the present paper), required an $M_{up} = 80 M_{\odot}$, while their model computed by matching the O/H values from collisionally excited lines (or DM, in the present paper), required an $M_{up} = 40 M_{\odot}$.

The absolute value of current O/H(R) could be reproduced by CEMs that use stellar yields and IMFs different to those assumed in this paper; nevertheless, those CEMs could not reproduce the chemical history of the solar vicinity, that is, the abundance ratios shown by stars of diverse ages in our neighborhood, including the Sun. Moreover, with those sets, the star formation history may change, and consequently the fitting to the metal distribution functions would change. In any case, even if one assumes other sets of yields and IMFs, other M_{up} values would be required, but always $M_{up}(TIM) > M_{up}(DM)$, because the O/H values determined from the TIM are higher than those from the DM.

Mollá et al. (2015) tested stellar yields and IMFs using 144 CEMs, all built to reproduce the solar abundances. They found 4 best models that reproduce: i) for the Galactic disk, the radial distribution of the gas mass, stellar mass, SFR, C/H, N/H, and O/H; and ii) for the solar vicinity, the SFR and [Fe/H] evolutions, the $[\alpha/Fe]$ vs [Fe/H] trend and the metal distribution function, both for $[Fe/H] < 0$. Unfortunately, they cannot achieve neither the $[\alpha/Fe]$ nor the [Fe/H] values observed in the most metal rich stars ($[Fe/H] > 0$) of the solar vicinity, because the O/H gradient used as observational constraint presents a mean dispersion of ~ 0.6 dex at the solar galactocentric radius. It is worth to note that all their best models consider the IMF by Kroupa (2002) (identical for $m > 0.08 M_{\odot}$ to the Kroupa et al. 1993, IMF used in our models).

Mishurov & Tkachenko (2018) have produced a Galactic disk model to fit the Cepheids O/H values obtained by Martin et al. (2015). Their model is in agreement with the H II region O/H values derived with the TIM abundances in the 7-14 kpc range. For $R < 7$ kpc their predicted O/H values become higher than the observed ones, as much as $\sim 0.3dex$.

In this work, we propose a simple formula of inside-out quenching of the SFR, as one of the processes that produces an O/H flattening; there are other, more complex, formulas able to produce a similar drop in the inner O/H gradient. We need ages and chemical abundances of stars located in the inner galactocentric radii to confirm the flattening and the validity

of this quenching formula. Moreover, cosmological simulations and dynamical models could give some hints to other flattening formulas and other possible alternatives. However, our simple formula can reproduce the color gradients present in local galaxies (e.g. Lian et al. 2017) and in spiral galaxies located in the transition region between star forming galaxies and quiescent ones (Belfiore et al. 2017).

In a recent work, Esteban & García-Rojas (2018, see also references therein) mentioned some possible reasons behind the star formation quenching: a gas depletion in the inner disk induced by the Galactic bar, or an increase of the gas turbulence within the bar-corotation radius (3.4 – 7 kpc). However, they compared the flattening radius of the O/H gradient in the MW ($R \sim 6$ kpc) with the inner-drop radius in the O/H gradient of other galaxies; this drop occurs at about one half the effective radius (that corresponds to $R \sim 2$ kpc for the MW); although 6 kpc is within the estimated value for the corotation radius of the MW bar, it is much larger than what is observed in other galaxies (Sánchez-Menguiano et al. 2018).

In particular, between 3 and 6 kpc, we increased the amount of accreted gaseous mass, and did not incorporate this extra fresh gas to the SFR. For these models to reproduce the O/H, the predicted current gas mass in the inner disk, is higher than observed (by ~ 0.2 and 0.3 dex for values from TIM and DM methods, respectively).

To test for alternatives to explain the O/H flattening we explored dilution models without changing the star formation history. Extreme dilution models can produce any flattening we require, since an accretion of primordial gas can increase the H abundance significantly. In particular, between 3 and 6 kpc, we increased the amount of accreted gaseous mass, and did not incorporate this extra fresh gas to the SFR. For these models to reproduce the O/H, the predicted current gas mass in the inner disk, is higher than observed, by about a factor of 2, and the required infall at present time is more than 3 orders of magnitude larger than what is observed.

Based on the current set of O/H data from H II regions, B-stars, and young Cepheids we cannot conclude if the gradient for $R < 6$ kpc is steep or flat. For this reason, we present the CP11 and TIM models, the first one was built to reproduce a steep inner gradient and the second model, to match a flat gradient. The TIM model explains the O/H flattening as a consequence of an abrupt decline of the star formation rate from 3 to 5 kpc, and from ~ 4.1 to 8.4 Gyr, as a consequence of an inside-out star formation quenching.

Some recent chemical and chemodynamical models for the Galactic disk do not seem to produce a flat inner O/H gradient, by considering radial migration of gas and/or stars induced mainly by the Galactic bar. Cavichia et al. (2014) obtained a very steep O/H gradient in the 4 - 8 kpc range, contrary to the observations. Minchev et al. (2014) predicted

a steep O/H gradient for $R < 10$ kpc, even steeper than the CP11 gradient for $R < 5$ kpc. Kubryk et al. (2015b) achieved a flat gradient, but only for the 3 to 4 kpc range.

6. Summary and Conclusions

The temperature independent method (the one based on the recombination lines of O and H), produces O/H values that are systematically higher than those derived from the direct method (the one based on the temperature derived from the ratio of the auroral to nebular lines of O). The abundance discrepancy between these 2 methods can be explained by the existence of temperature inhomogeneities, that undermine the basic assumptions of the DM determinations producing lower O/H values than the TIM ones.

The correction of the O/H values due to the temperature inhomogeneities is about 2 times higher than the correction due to the fraction of O embedded in dust grains.

A parabolic fit in the 5 to 18 kpc range is better than a linear fit for the log O/H versus R distribution. Therefore we expect a flatter O/H gradient in the inner parts than in the outer parts of the disk for H II regions and for recently formed stars, those with ages smaller than about 0.5 Gyr.

We present two galactic chemical evolution models, one that fits the O/H values in H II regions based on the DM, and another that fits the O/H values based on the TIM. We also discuss the model by Carigi & Peimbert (2011) that is in excellent agreement with the model that fits the O/H values based on the TIM for the 6 to 18 kpc range.

The current O/H abundances derived from the TIM chemical evolution model are in excellent agreement with the observations of: a) Cepheids, b) early B type stars, and c) the Sun (after modeling the chemical evolution of the Galaxy since the Sun was formed). The ability to reproduce the chemistry present when the Sun was formed, as well as the current chemical gradient show the capacity of the TIM model to reproduce the last 5 Gyrs of galactic chemical evolution.

On the other hand, the current O/H abundances derived from the DM chemical evolution model are typically smaller by about 0.25 dex than those observed in: a) Cepheids, b) early B type stars, and c) the Sun (after modeling the chemical evolution of the Galaxy since the Sun was formed), regardless of the stellar migration assumed for the Sun.

As expected, the TIM model presented in this paper is in excellent agreement with the abundances derived in the 6 to 18 kpc range. However, more abundance determinations are needed in the 3 to 6 kpc range to discriminate between the CP11 and TIM models.

If the flattening of the O/H ratio range is corroborated, it would imply an inside-out star formation rate quenching in the 3-5 kpc range starting ~ 9 Gyrs ago.

We are grateful to R. Pierre Martin, César Esteban and Sebastián Sánchez for pertinent letters and many fruitful discussions. We are also grateful to the referee for many relevant suggestions that improved this paper. We would like to acknowledge support from CONA-CyT, grant 247132; L.C. also received partial support from PAPIIT (DGAPA-UNAM), grants no. IG100115, IA101215, and IA101517) as well as partial support from MINECO (Spain), grant no. AYA2015-65205-P; A.P acknowledge support from PAPIIT (DGAPA-UNAM), grant no. IN109716.

REFERENCES

- Andrievsky, S. M., Martin, R. P., Kovtyukh, V. V., Korotin, S. A., & Lépine, J. R. D. 2016, MNRAS, 461, 4256
- Asplund, M., Grevesse, N., Sauval, A. J., & Scott, P. 2009, ARA&A, 47, 481
- Belfiore, F., Maiolino, R., Maraston, C. et al. 2017, MNRAS, 466, 2570
- Berg, D. A., Skillman, E. D., Henry, R. B. C., Erb, D. K., & Carigi, L. 2016 ApJ, 827, 126
- Bresolin, F., Gieren, W., Kudritzki, R.-P., et al. 2019, ApJ, 700, 309
- Bresolin, F., Kudritzki, R.-P., Urbaneja, M. A., et al. 2016, ApJ, 830, 64
- Carigi, L. & Hernandez, X., 2008, MNRAS, 390, 582
- Carigi, L. & Peimbert, M., 2008, RMxAA., 44, 341
- Carigi, L. & Peimbert, M., 2011, RMxAA, 47, 139
- Cavichia, O., Mollá, M., Costa, R. D. D., & W. J. Maciel, W. J., 2014, MNRAS, 437, 3688
- Chiappini, C., Matteucci, F., & Gratton R. 1997, ApJ, 477, 765
- Côté, B., Ritter, C., O’Shea, B. W., Herwig, F., Pignatari, M., Jones, S., Fryer, C. L. 2016, ApJ, 824, 82
- Espíritu, J. N., Peimbert, A. Delgado-Inglada, G., & Ruiz, M. T. 2017, RMxAA, 53, 95
- Esteban, C., Carigi, L., Copetti, M. V. F., García-Rojas, J., Mesa-Delgado, A., Castañeda, H. O., & Péquignot, D. 2013, MNRAS, 433, 382

- Esteban, C., Fang, X., García-Rojas, J., & Toribio San Cipriano, L. 2017, MNRAS, 471, 987
- Esteban, C., García-Rojas, J., Peimbert, M., Peimbert, A., Ruiz, M. T., Rodríguez, M., & Carigi, L., 2005, ApJ, 618, L95
- Esteban, C., & García-Rojas, J., 2018, MNRAS, 478, 2315
- Esteban, C., Mesa-Delgado, A., Morisset, C., & García-Rojas, J. 2016, MNRAS, 460, 2038
- Esteban, C., Peimbert, M., García-Rojas, J., Ruiz, M. T., Peimbert, A., & Rodríguez, M. 2004 MNRAS, 355, 229
- Fernández-Martín, A., Pérez-Montero, E., Vílchez, J. M., & Mampaso, A. 2017, A&A, 597, A84
- Fenner, Y., & Gibson, B. K. 2003, PASA, 20, 189
- García-Rojas, J., Esteban, C., Peimbert, A., Peimbert, M., Rodríguez, M., & Ruiz, M. T. 2005, MNRAS, 362, 301
- García-Rojas, J., Esteban, C., Peimbert, A., Rodríguez, M., Ruiz, M. T. Peimbert, M., & Ruiz, M. T. 2007, RMxAA, 43, 3
- García-Rojas, J., Esteban, C., Peimbert, M., Costado, M. T., Rodríguez, M., Peimbert, A., & Ruiz, M.T., 2006, MNRAS, 368, 253
- García-Rojas, J., Esteban, C., Peimbert, M., Rodríguez, M., Ruiz, M. T., & Peimbert, A. 2004, ApJS, 153, 501
- García-Rojas, J., Simón-Díaz, S., & Esteban, C. 2014, A&A, 571, A93
- Greggio, L. & Renzini, A. 1983, A&A, 118, 217
- Hayden, M. R., Bovy, J., Holtzman, J. A. et al. 2015, ApJ, 808, 132
- Hernández-Martínez, L., Carigi, L., Peña, M., Peimbert, M. 2011, A&A, 535, 118
- Hirschi, R. 2007, A&A, 461, 571
- Kennicutt, R. C. 1998, ApJ, 498, 541
- Kennicutt, R. C. & Evans, N. J. 2012, ARA&A, 50, 531
- Korotin, S. A., Andrievsky, S. M., Luck, R. E., Lépine, J. R. D., Maciel, W. J., & Kovtyukh, V. V. 2014, MNRAS, 444, 3301

- Kroupa, P., Tout, C. A., & Gilmore, G. 1993, MNRAS, 262, 545
- Kubryk, M., Prantzos, N., & Athanassoula, E. 2015a, A&A, 580, A126
- Kubryk, M., Prantzos, N., & Athanassoula, E. 2015b, A&A, 580, A127
- Lian, J., Yan, R., Blanton, M., & Kong, X. 2017 MNRAS, 472, 4679
- Luck, R. E., Andrievsky S. M., Korotin S. N., & Kovtyukh V. V., 2013, AJ, 146, 18
- Luck, R. E. & Lambert, D. L. 2011, AJ, 142, 137
- Maeder A., 1992, A&A, 264, 105
- Marigo, P., Bressan, A., & Chiosi, C., 1996, A&A, 313, 545
- Marigo, P., Bressan, A., & Chiosi, C., 1998, A&A, 331, 564
- Martin, R. P., Andrievsky, S. M., Kovtyukh, V. V., Korotin, S. A., Yegorova, I. A., & Saviane, I. 2015, MNRAS, 449, 4071
- Martínez-Medina, L. A., Pichardo, B., Peimbert, A., & Carigi, L. 2017, MNRAS, 468, 3615
- Matteucci, F., & Chiappini, C. 1999, in Chemical Evolution from Zero to High Redshift, ed. J. R. Walsh & M. R. Rosa (Berlin: Springer-Verlag), 83
- Meynet, G., & Maeder, A. 2002, A&A, 390, 561
- Minchev, I., Chiappini, C. & Martig, M., 2013, A&A 558, A9
- Minchev, I., Chiappini, C. & Martig, M., 2014, A&A 572, A92
- Mishurov, Yu. N. & Tkachenko, V. 2018, MNRAS, 473, 3700
- Mollá, M., Cavichia, O., Gavilán, M., and Gibson, B. K. 2015, MNRAS, 451, 3693
- Mollá, M., Díaz, A. I., Gibson, B. K., Cavichia, O., López-Sánchez, A. R. 2016 MNRAS, 462, 1329
- Nieva, M.-F. & Simón-Díaz, S. 2011, A&A, 532, 2
- Nieva, M.-F. & Przybilla, N. 2012, A&A, 539, A143
- Nomoto, K., Iwamoto, K., Nakasato, N., Thielemann, F.-K., Brachwitz, F., et al. 1997, Nucl. Phys. A., 621, 467

- Nuza, S. E., Scannapieco, C., Chiappini, C., Junqueira, T. C., Minchev, I., & Martig, M. 2018 MNRAS, submitted (arXiv:1805.06428)
- Peimbert, A. & Peimbert, M. 2010, ApJ, 724, 791
- Peimbert, M., 1967, ApJ, 151, 825
- Peimbert, M. & Costero, R. 1969, BOTT, 5, 3
- Peimbert, M., Peimbert, A., & Delgado-Inglada, G. 2017, PASP, 129,082001
- Peña-Guerrero, M. A., Peimbert, A., & Peimbert, M. 2012, ApJ, 756, L14
- Pérez-Montero, E. 2017, PASP, 129, 03001
- Portinari, L., Chiosi, C., & Bressan, A., 1998, A&A, 334, 505
- Portegies Zwart S. F., 2009, ApJ, 696, L13
- Prantzos, N. 2016, Astronomische Nachrichten, 337, 953
- Renda, A., Kawata, D., Fenner, Y. and Gibson. B. K. 2005, MNRAS, 356, 1071
- Robles-Valdez, F., Carigi, L., Peimbert, M. 2013, MNRAS, 429, 2351
- Rolleston, W. R. J., Smartt, S. J., Dufton, P. L., & Ryans, R. S. I. 2000, A&A, 363, 537
- Rudolph, A. L., Fich, M., Bell, G. R., et al. 2006, ApJS, 162, 346
- Romano, D., Chiappini, C., Matteucci, F., and Tosi, M. 2005, A&A, 430, 491
- Romano, D., Karakas, A. I., Tosi, M., and Matteucci, F. 2010, A&A, 522, A32
- Sánchez-Menguiano, L., Sánchez, S. F., Pérez, I., Ruiz-Lara, T, Galbany, L., et al. 2018, A&A, 609, 119
- Shi, Y., Yan, L., Armus, L., Gu, Q., Helou, G., Qiu, K., Gwyn, S., Stierwalt, S., Fang, M., Chen, Y. et al., 2018, ApJ, 853, 149
- Smartt, S. J., Venn, K. A., Dufton, P. L., et al., 2001, A&A, 367, 86
- Toribio San Cipriano, L., García-Rojas, J., Esteban, C., Bresolin, F., & Peimbert, M., 2016, MNRAS, 458, 1866
- Wielen, R., Fuchs, B., & Dettbarn, C., 1996, A&A, 314, 438

Woosley, S. E. & Weaver, T. A., 1995, *ApJS*, 101, 181

Yin, J., Hou, J. L., Prantzos, N., Boissier, S., Chang, R. X., Shen, S. Y., & Zhang, B., 2009, *A&A*, 505, 497

Table 1. Forbidden O/H abundances for $t^2 = 0.00$ and including dust

Name	R (kpc)	O/H_{FL}	$O/H_{\text{FL}} + \text{DUST}^{\text{a}}$	Source ^b
M 20	5.1 ± 0.3	8.51 ± 0.04	8.62 ± 0.05	(1, 2)
M 16	5.9 ± 0.2	8.54 ± 0.04	8.65 ± 0.05	(1, 2)
M 17	6.1 ± 0.2	8.54 ± 0.04	8.65 ± 0.05	(1, 3)
M 8	6.3 ± 0.8	8.45 ± 0.04	8.56 ± 0.05	(1, 3)
NGC 3576	7.5 ± 0.3	8.55 ± 0.04	8.66 ± 0.05	(1, 4)
IC 5146	8.10 ± 0.02	8.56 ± 0.04	8.67 ± 0.05	(1, 5)
M 42	8.34 ± 0.02	8.50 ± 0.04	8.61 ± 0.05	(1, 6)
NGC 3603	8.6 ± 0.4	8.44 ± 0.03	8.55 ± 0.04	(1, 2)
Sh 2-100	9.4 ± 0.3	8.52 ± 0.03	8.63 ± 0.04	(1)
Sh 2-132	10.0 ± 0.7	8.35 ± 0.14	8.46 ± 0.14	(1, 7)
NGC 7635	10.2 ± 0.7	8.40 ± 0.08	8.51 ± 0.08	(1, 8)
Sh 2-156	10.6 ± 0.6	8.32 ± 0.10	8.43 ± 0.10	(1, 7)
Sh 2-311	11.1 ± 0.4	8.39 ± 0.01	8.50 ± 0.03	(1, 9)
Sh 2-298	11.9 ± 0.7	8.41 ± 0.02	8.52 ± 0.03	(1)
NGC 2579	12.4 ± 0.5	8.26 ± 0.03	8.36 ± 0.04	(1, 10)
Sh 2-128	12.5 ± 0.4	8.19 ± 0.03	8.29 ± 0.04	(1)
Sh 2-288	14.1 ± 0.4	8.31 ± 0.08	8.42 ± 0.08	(1)
Sh 2-127	14.2 ± 1.0	8.25 ± 0.04	8.35 ± 0.05	(1)
Sh 2-212	14.6 ± 1.4	8.15 ± 0.12	8.25 ± 0.12	(1)
Sh 2-83	15.3 ± 0.1	8.14 ± 0.05	8.24 ± 0.06	(1)
Sh 2-209	17.0 ± 0.7	8.09 ± 0.10	8.19 ± 0.10	(1)

^aThe dust contribution is based on Peimbert & Peimbert (2010), Peña-Guerrero et al. (2012), and Espíritu et al. (2017).

^b(1) Esteban et al. (2017); sources for $(O/H)_{\text{FL}}$ values: (1) Esteban et al. (2017), (2) García-Rojas et al. (2006), (3) García-Rojas et al. (2007), (4) García-Rojas et al. (2004), (5) García-Rojas et al. (2014), (6) Esteban et al. (2004), (7) Fernández-Martín et al. (2017), (8) Esteban et al. (2016), (9) García-Rojas et al. (2005), (10) Esteban et al. (2013).

Table 2. Recombination O/H abundances corrected for dust

Name	R (kpc)	O/H _{RL}	O/H _{RL} + DUST ^a	Source ^b
M 20	5.1±0.3	8.71±0.07	8.82±0.08	(1)
M 16	5.9±0.2	8.81±0.07	8.92±0.08	(1)
M 17	6.1±0.2	8.76±0.04	8.87±0.05	(2)
M 8	6.3±0.8	8.71±0.04	8.82±0.05	(2)
NGC 3576	7.5±0.3	8.74±0.06	8.85±0.07	(3)
M 42	8.34±0.02	8.65±0.03	8.76±0.04	(4)
NGC 3603	8.6±0.4	8.72±0.05	8.83±0.06	(1)
Sh 2-100	9.4±0.3	8.58±0.05	8.69±0.06	(5)
Sh 2-311	11.4±0.4	8.57±0.05	8.68±0.06	(6)
NGC 2579	12.4±0.5	8.56±0.03	8.67±0.05	(7)

^aThe dust contribution is based on Peimbert & Peimbert (2010), Peña-Guerrero et al. (2012), and Espíritu et al. (2017).

^b(1) García-Rojas et al. (2006), (2) García-Rojas et al. (2007), (3) García-Rojas et al. (2004), (4) Esteban et al. (2004), (5) Esteban et al. (2017), (6) García-Rojas et al. (2005), (7) Esteban et al. (2013).

Table 3. Forbidden O/H abundances corrected for dust and temperature inhomogeneities

Name	R (kpc)	$O/H_{\text{FL}}, t^2 = 0.00$	O/H_{TOTAL}
IC 5146	8.10 ± 0.02	8.56 ± 0.04	8.89 ± 0.06
Sh 2-132	10.0 ± 0.7	8.35 ± 0.14	8.76 ± 0.15
NGC 7635	10.2 ± 0.7	8.40 ± 0.08	8.72 ± 0.09
Sh 2-156	10.6 ± 0.6	8.32 ± 0.10	8.63 ± 0.11
Sh 2-298	11.9 ± 0.7	8.41 ± 0.02	8.73 ± 0.05
Sh 2-128	12.5 ± 0.4	8.19 ± 0.03	8.49 ± 0.06
Sh 2-288	14.1 ± 0.4	8.31 ± 0.08	8.62 ± 0.09
Sh 2-127	14.2 ± 1.0	8.25 ± 0.04	8.56 ± 0.06
Sh 2-212	14.6 ± 1.4	8.15 ± 0.12	8.45 ± 0.13
Sh 2-83	15.3 ± 0.1	8.14 ± 0.05	8.44 ± 0.07
Sh 2-209	17.0 ± 0.7	8.09 ± 0.10	8.38 ± 0.12

The R and O/H_{FL} values for $t^2 = 0.00$ come from Table 1. The O/H_{TOTAL} values include the t^2 effect and the dust correction based on the calibration by Peña-Guerrero et al. (2012). Therefore the O/H_{TOTAL} values are equivalent to the $O/H_{\text{RL}} + \text{DUST}$ values.

Table 4. Comparison of O/H gradients for different radial intervals

R Interval (kpc)	$\Delta \log(\text{O}/\text{H})/\Delta R$ other papers	Equation (2) this paper	Object	Source
6–11	-0.044 ± 0.010	-0.0349	H II Regions	(1)
11–17	-0.046 ± 0.017	-0.0654	H II Regions	(2)
11–18	-0.053 ± 0.009	-0.0678	H II Regions	(3)
5–18	-0.060	-0.0531	H II Regions	(4)
6–18	-0.067	-0.0556	B Stars	(5)
5–18	-0.058	-0.0531	Cepheids	(6)
5–17	-0.056	-0.0507	Cepheids	(7)

- (1) Esteban et al. (2005), (2) Esteban et al. (2017), (3) Fernández-Martín et al. (2017), (4) Rudolph et al. (2006), (5) Rolleston et al. (2000), (6) Korotin et al. (2014), (7) Luck & Lambert (2011).

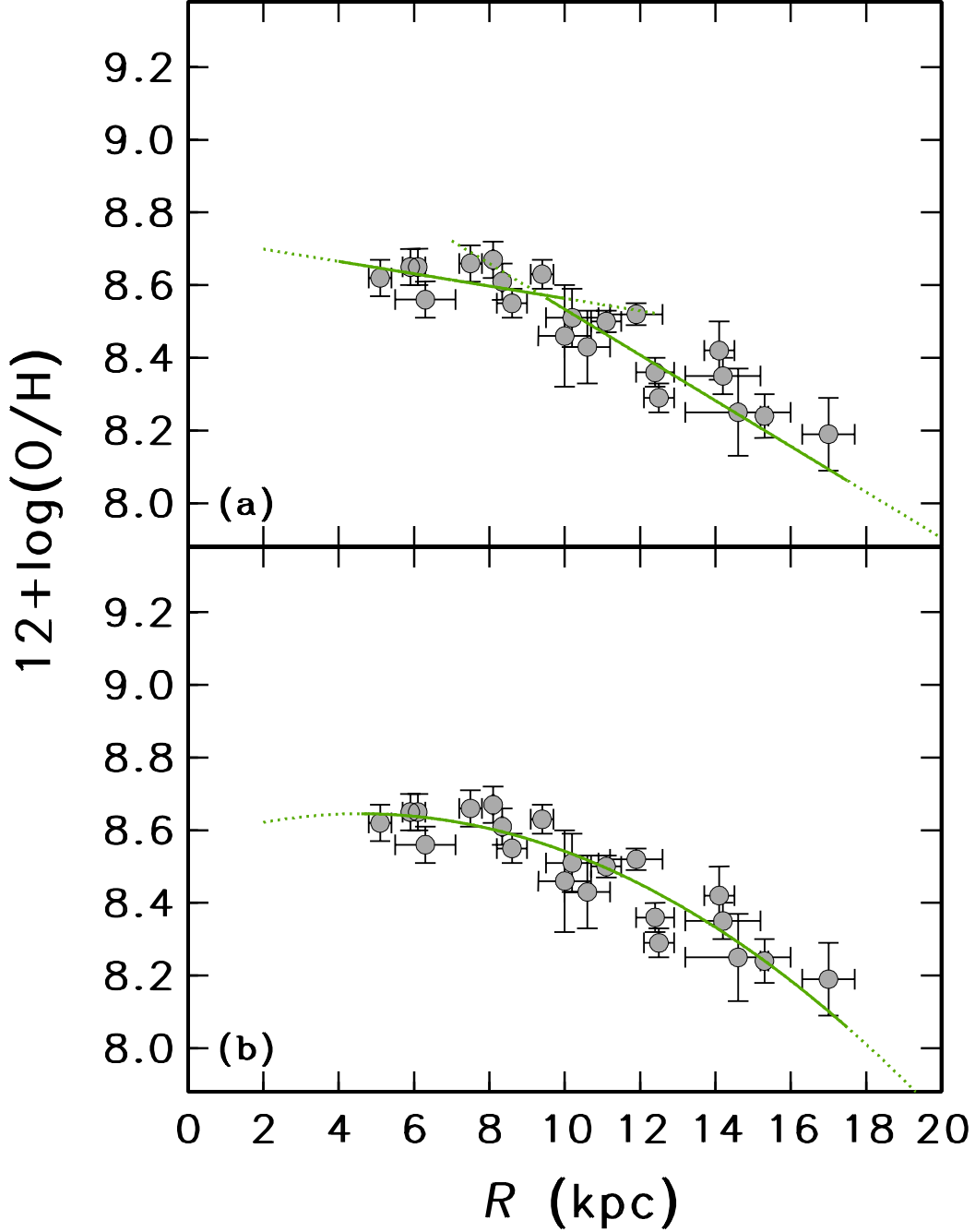


Fig. 1.— H II region O/H values obtained with the DM plus dust corrections versus the radial distance to the galactic center, R (see Table 1). The O/H values have been corrected by the fraction of O embedded in dust grains. In panel a the straight lines are the fits to the 4 - 10 kpc and the 9.5 - 17.5 kpc ranges and the slopes are: 0.0170 and 0.0629 dex/kpc, respectively. In panel b, a parabolic fit to the O/H values is shown the solid line corresponds to the analytic fit where data is available, the dotted lines correspond to extrapolations.

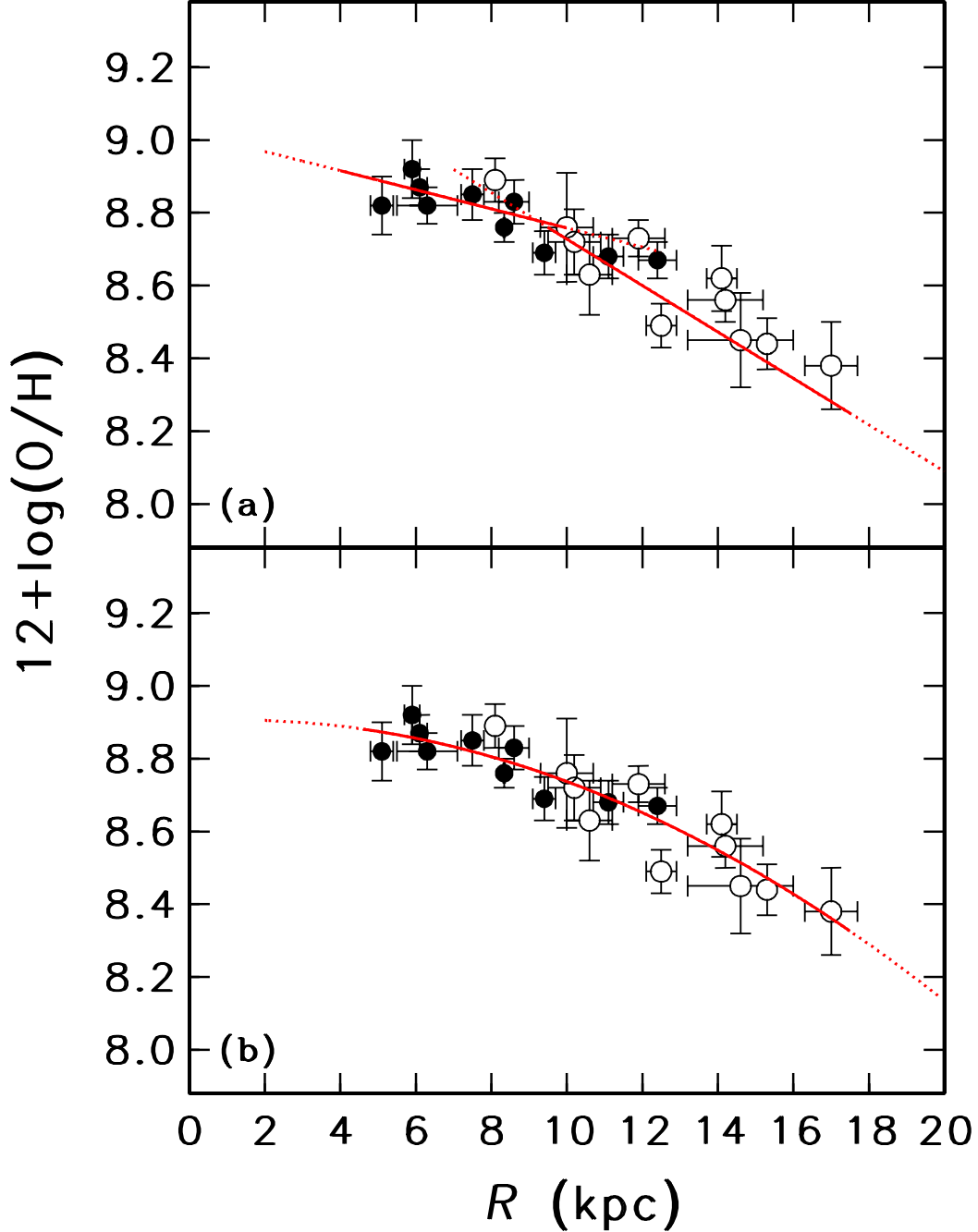


Fig. 2.— H II regions O/H values obtained with the TIM plus dust corrections versus the radial distance to the galactic center, R (see Table 3). The O/H values include the fraction of O embedded in dust grains. The straight lines are the fits to the 4 - 10 kpc and the 9.5 - 17.5 kpc ranges and the slopes are: 0.0263 and 0.0638, respectively. Parabolic fit to the O/H values obtained with the TIM. The filled circles denote direct observations of the recombination lines, the empty circles use the calibration by Peña-Guerrero et al. (2012). The solid line corresponds to the analytic fit where data is available, the dotted lines correspond to extrapolations.

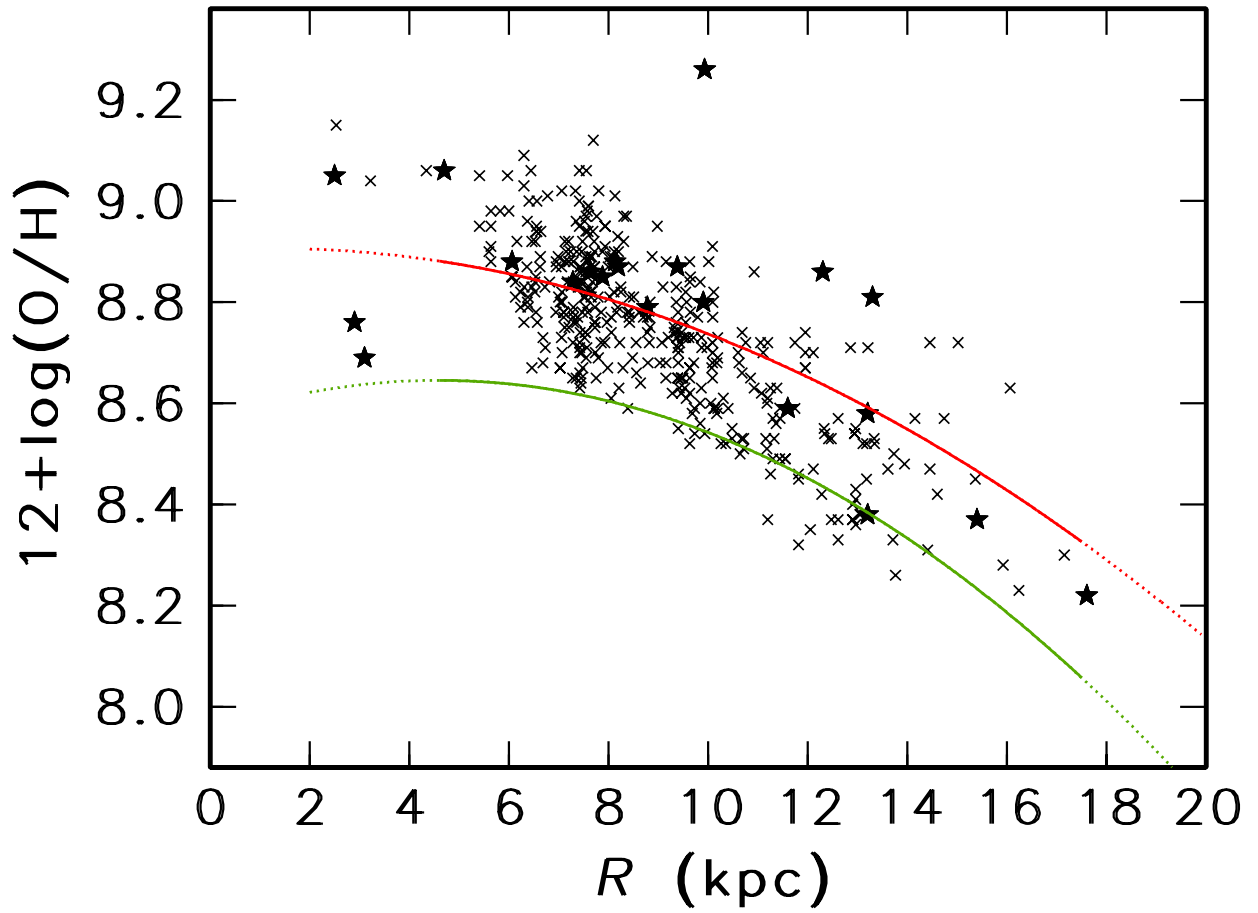


Fig. 3.— Parabolic fits of O/H for the DM (green) and the TIM (red) plus dust corrections together with the B-star data (stars; Rolleston et al. 2000; Smartt et al. 2001) and the Cepheid data (crosses; Martin 2017, private communication, see Section 3.3).

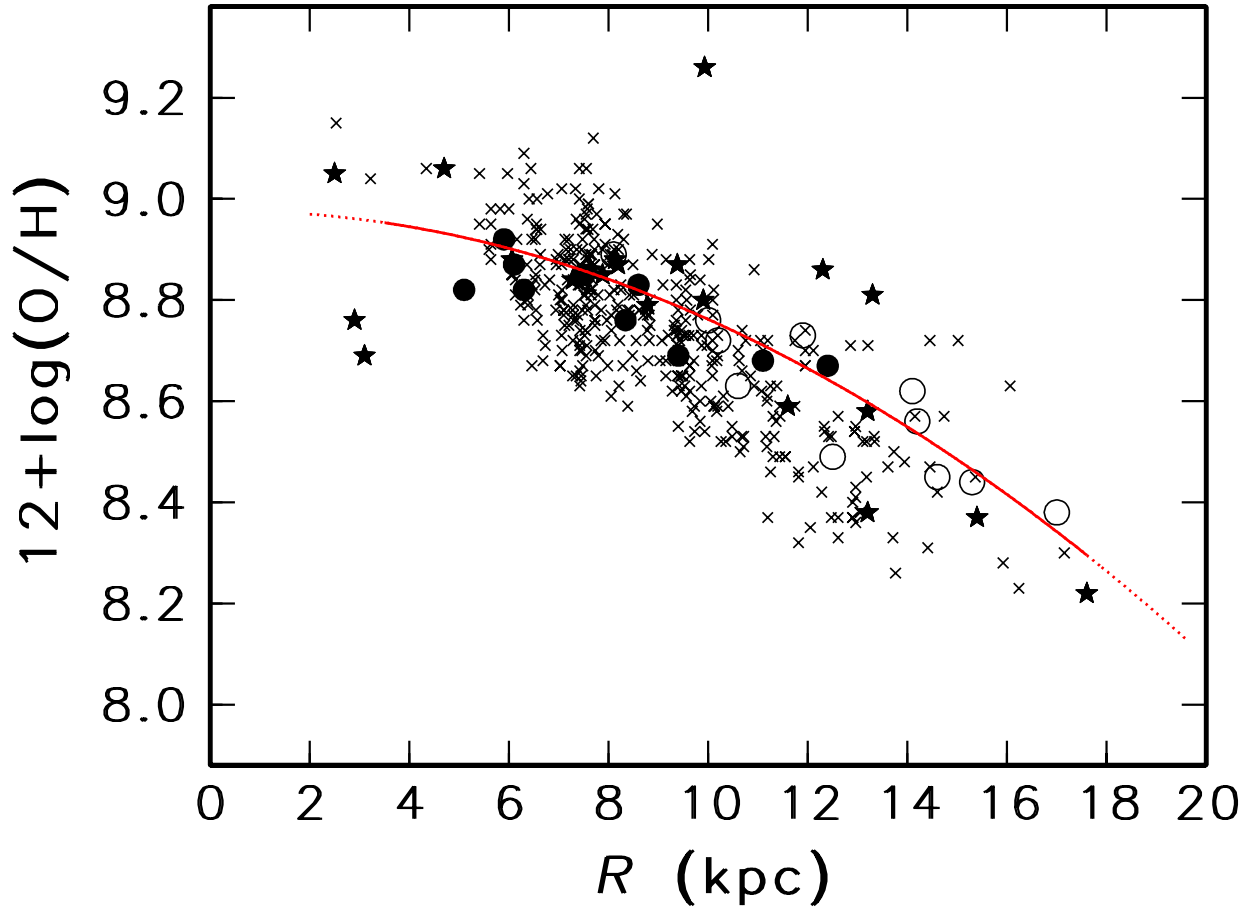


Fig. 4.— Parabolic fit of O/H averaging fits to the H II regions (circles; solid from RLs, empty from CELs corrected for t^2) plus dust corrections, to the B-star data (stars; Rolleston et al. 2000; Smartt et al. 2001), and to the Cepheid data (crosses; Martin 2017, private communication, see Section 3.3).

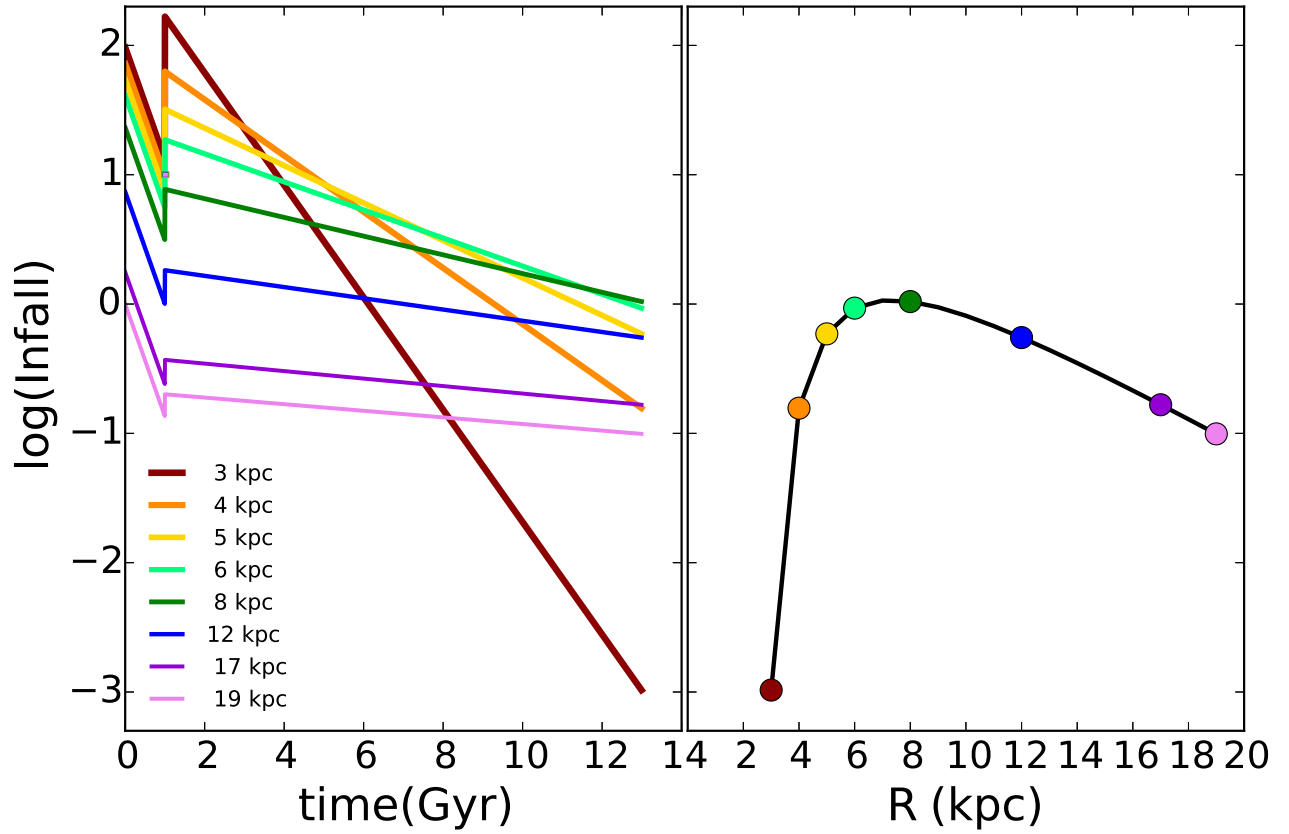


Fig. 5.— Evolution for different radii and present-day radial distribution of the infall, for the three models shown in this paper. Circles represent the infall at present day (13 Gyr). Colour circles as colour lines. Infall in $M_{\odot}\text{pc}^{-2}\text{Gyr}^{-1}$ units.

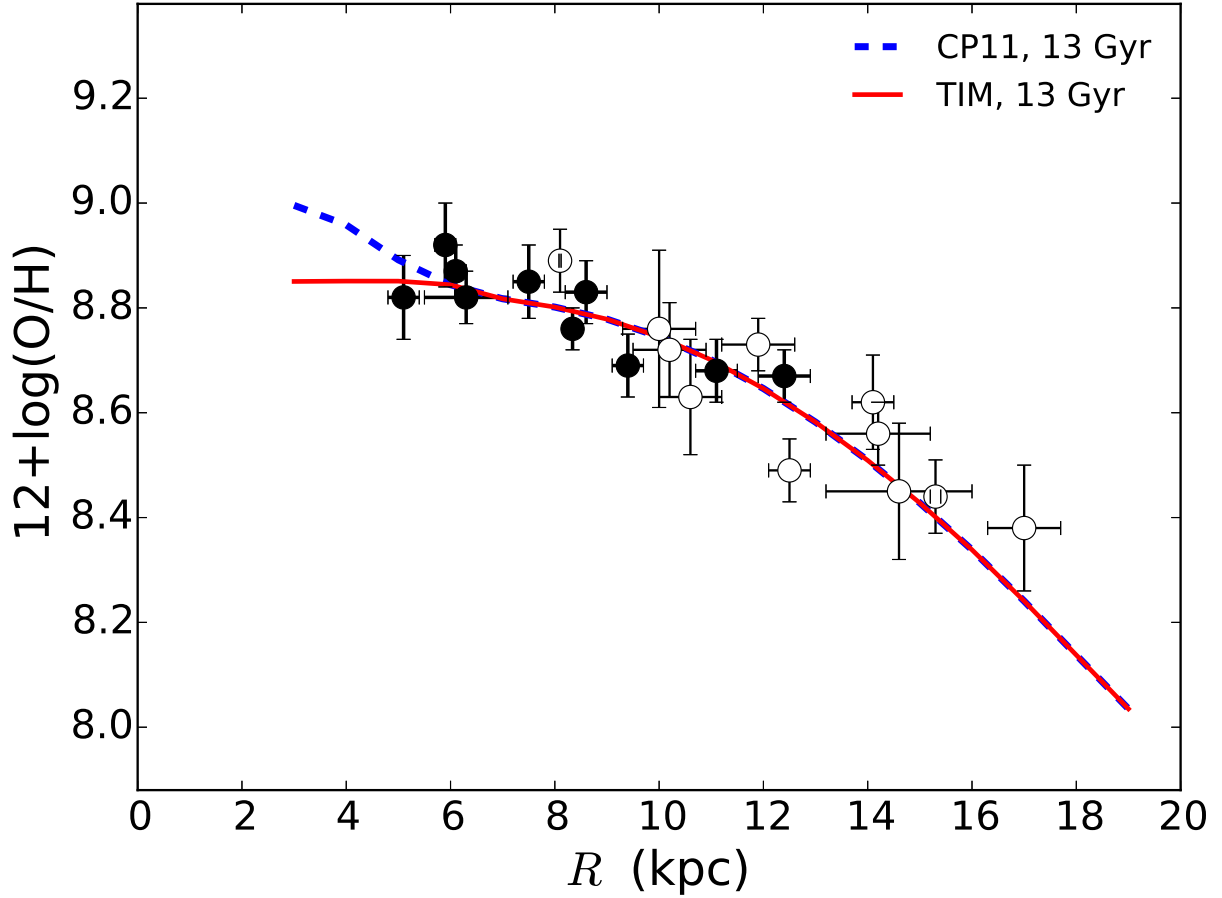


Fig. 6.— Current radial distribution of O/H obtained from the Galactic chemical evolution model by CP11 and from the model based on O/H values derived from the TIM plus dust corrections. Data as in Figure 2. CP11 model was made based only on the data obtained before 2012, but it provides an excellent fit to the data by Esteban et al. (2017) if one adopts the TIM.

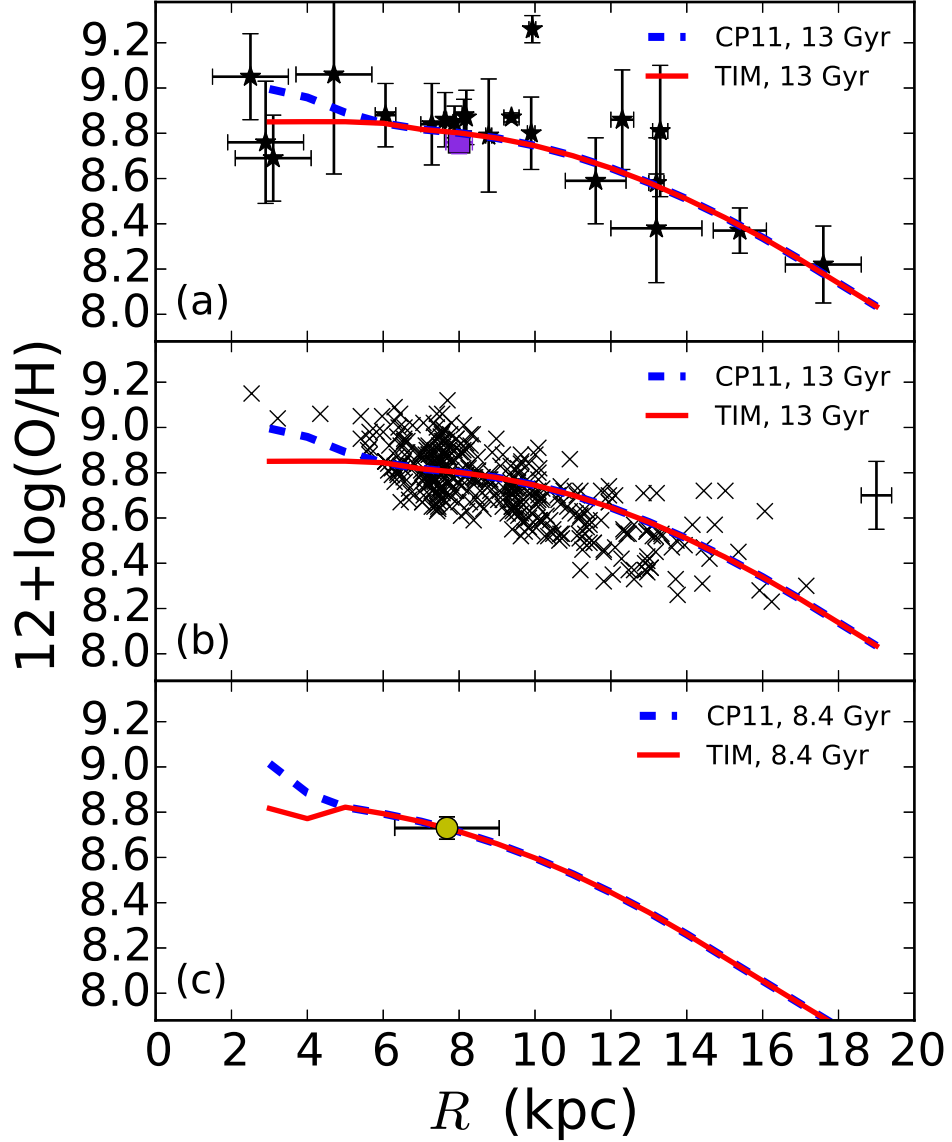


Fig. 7.— Radial distribution of O/H at present (13 Gyr) and at the Sun formation time (8.4 Gyr) obtained by CP11 and TIM models. Panel (a): B-stars by Rolleston et al. (2000) and Smartt et al. (2001), the violet square represents the average value and its standard deviation from B-stars by Nieva & Przybilla (2012). Panel (b): Cepheids as in Figure 3, the error bars presented near 19 kpc represent the uncertainty for the typical Cepheid. Panel (c): initial solar O/H value by Asplund et al. (2009) filled circle, the horizontal error bar in the O/H solar abundance represents the average migration of the Sun computed by Martínez-Medina et al. (2017).

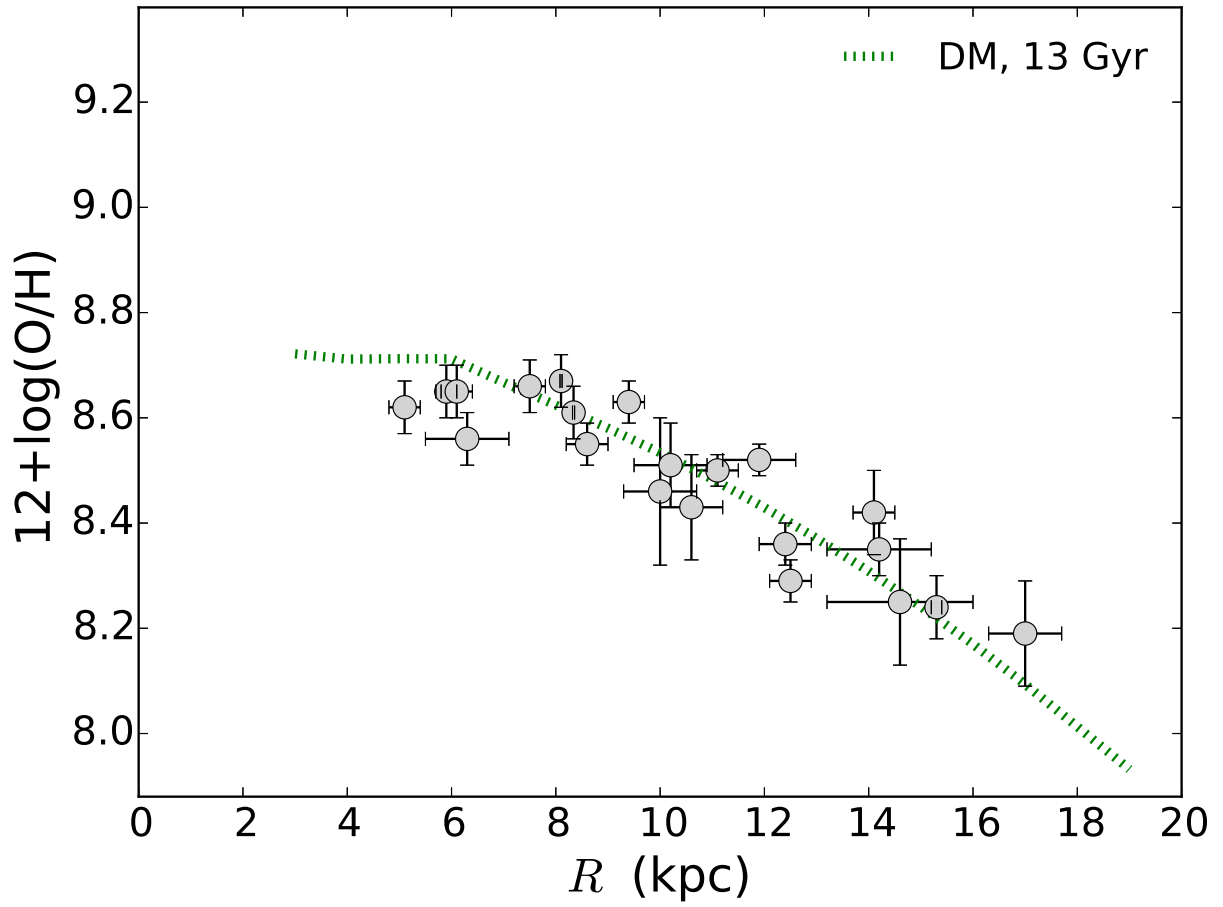


Fig. 8.— Current radial distribution of O/H obtained from the Galactic chemical evolution model based on the O/H values derived from the DM. Data as Figure 1.

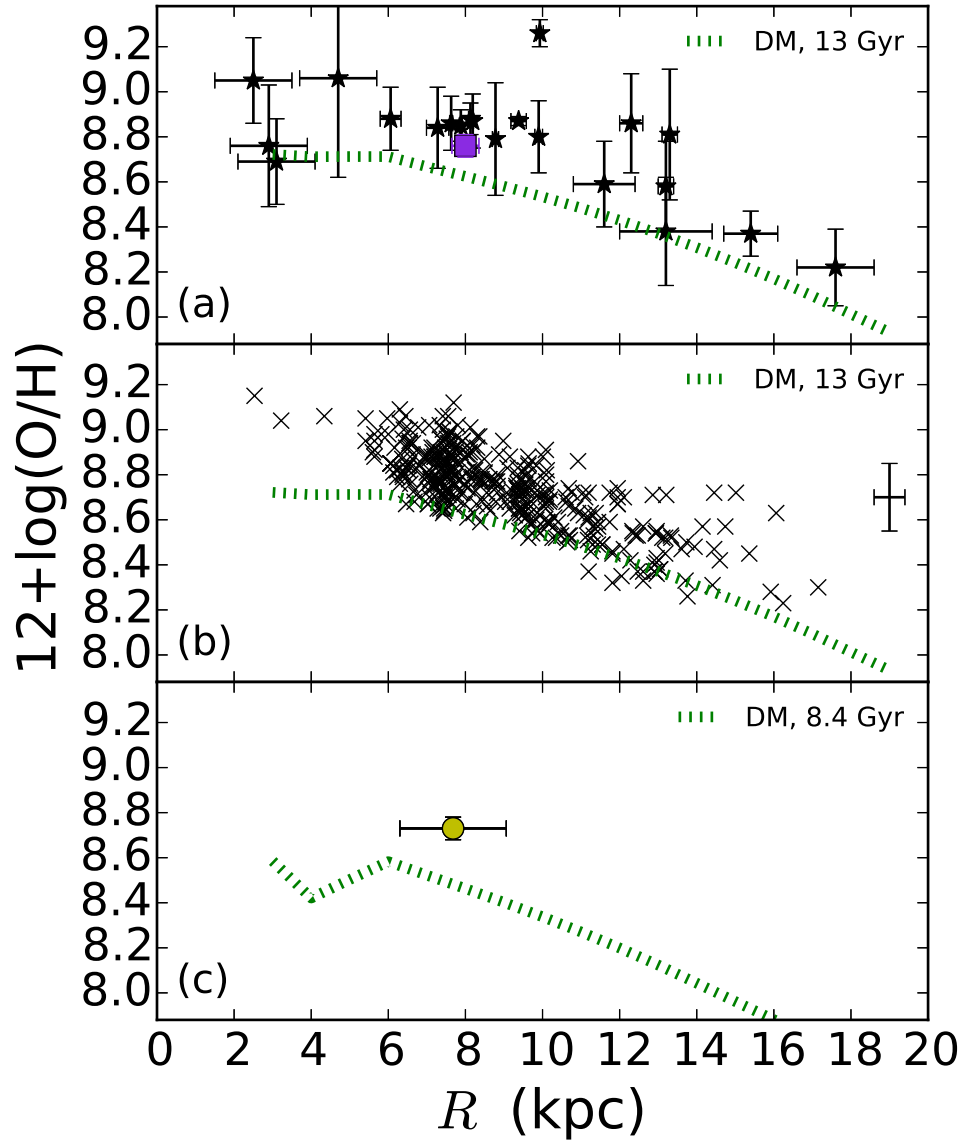


Fig. 9.— Same data as in Figure 7, but now compared with the model based on the DM.

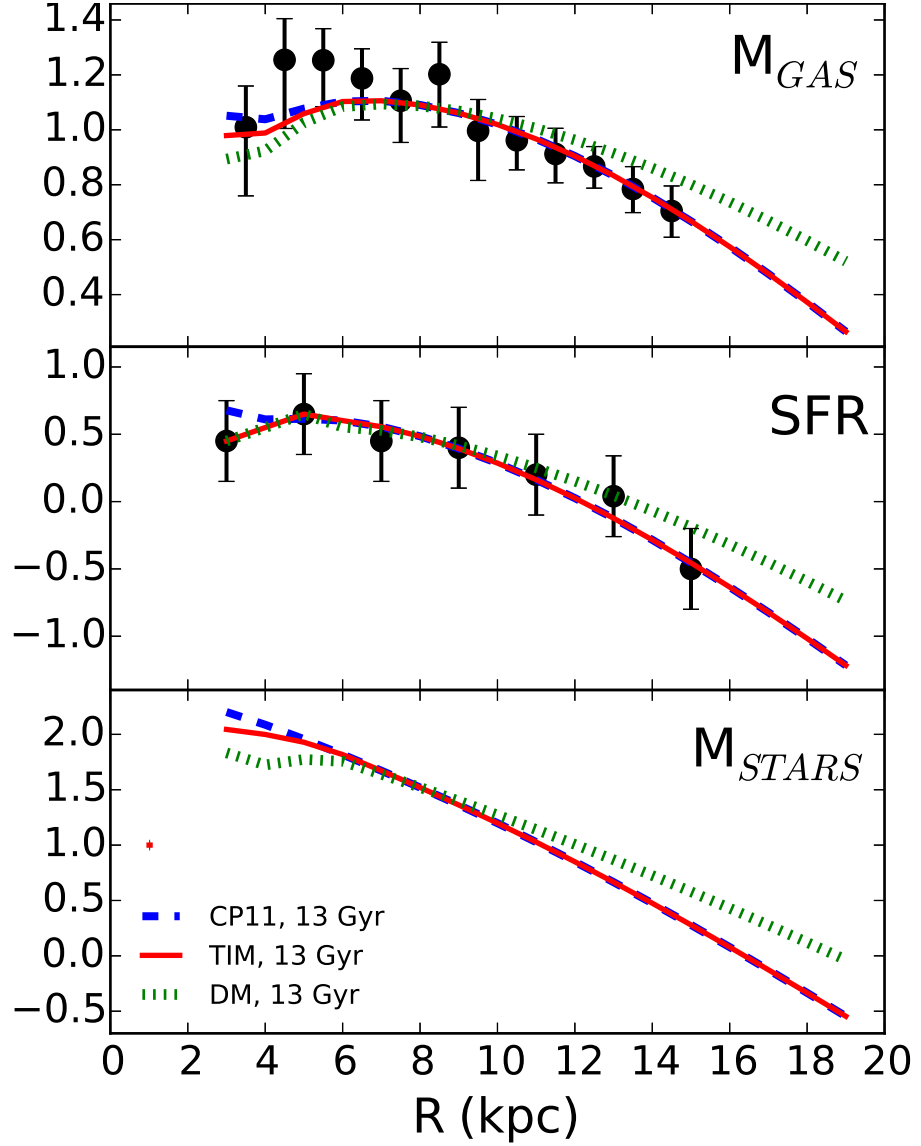


Fig. 10.— Current radial distribution of M_{gas} ($M_{\odot} \text{pc}^{-2}$), SFR ($M_{\odot} \text{pc}^{-2} \text{Gyr}^{-1}$), and M_{star} ($M_{\odot} \text{pc}^{-2}$) from CP11, TIM and DM models. Vertical axis in logarithmic scale. Observational data by Kennicutt & Evans (2012).

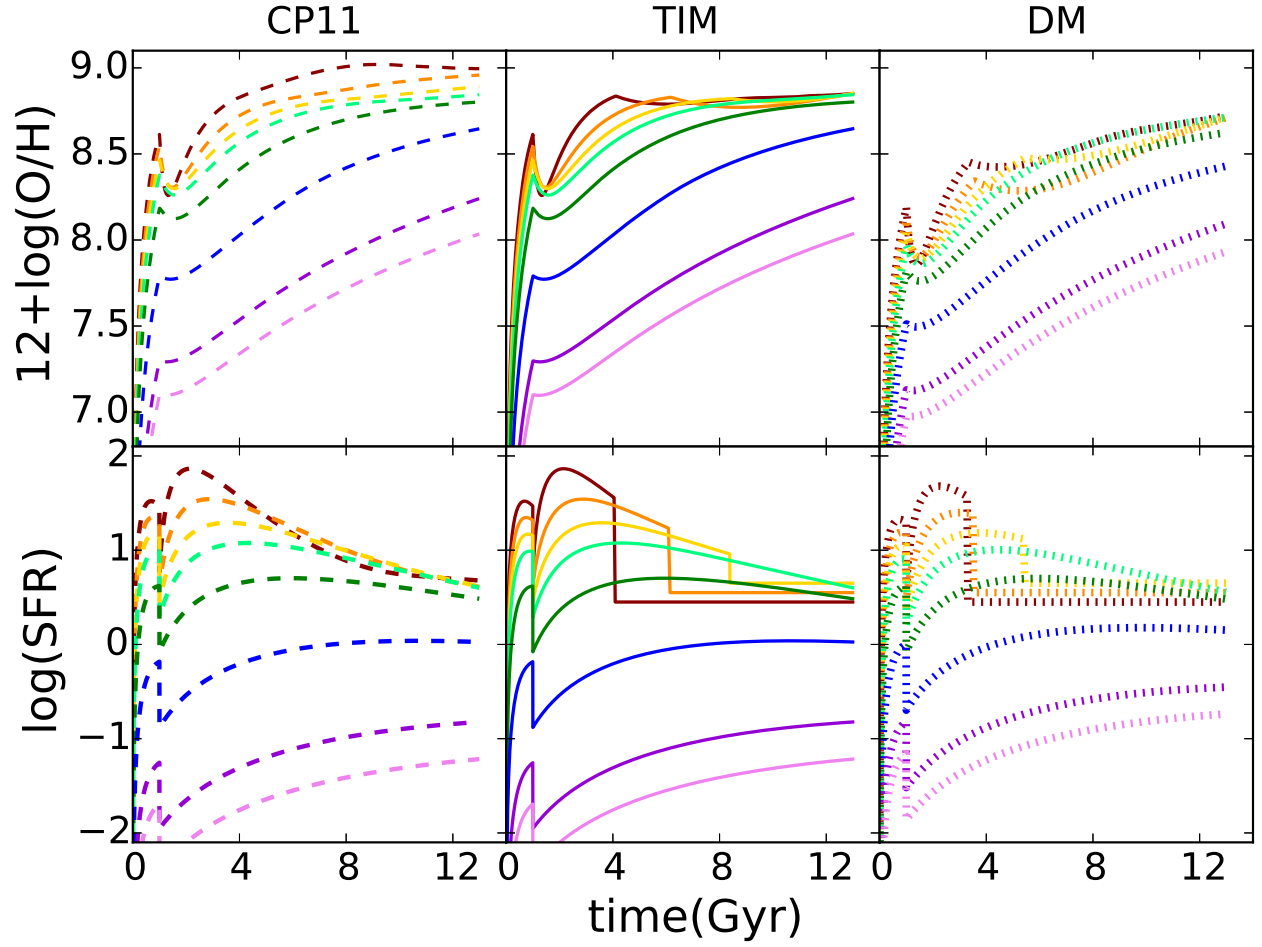


Fig. 11.— Evolution of O/H and star formation rate ($\text{M}_{\odot}\text{pc}^{-2}\text{Gyr}^{-1}$) inferred from CP11, TIM and DM models. Color lines represent different galactocentric radius, as Figure 5.